A 0.6-mm^2 Powering and Data Telemetry System Compatible with Ultrasound B-Mode Imaging for Freely Moving Biomedical Sensor Systems

Yihan Zhang and Kenneth L. Shepard
Department of Electrical Engineering, Columbia University, New York, NY

***Abstract*—A 0.6 mm^2 integrated circuit, fabricated in a 180 nm process, is designed to operate within the field of view of an ultrasound B-mode imager, allowing data to be received from ultra-small-form-factor devices that can be localized, powered, and configured as multiple freely moving ingestible or implantable systems. Power is harvested from ultrasound pulses emitted by the imaging transducer array and a bi-directional data link is established that is synchronized to the frame rate of the imager. The chip consumes 57 pW of power and supports data rates of 25 bit/s for uplink and 50 bit/s for downlink for an imager operating at 50 frames per second. Fully packaged within 11 mm^3 with a piezoelectric transducer, the chip enables tissue implants as deep as 71 mm. Real-time localizations of devices is possible within the field of view of the imager at 0.8-mm accuracy. An on-chip instruction set allows for software configuration and a smooth transition to a more power-intensive mode of operation using focused ultrasound pulses after localization, with 280 nW power delivery verified using 0.5% duty cycle ultrasound.**

Keywords—ultrasound; brightness mode imaging; localization; ingestible implants; backscatter

I. Introduction

There is a need for implanted or ingested medical devices that are freely moving in the body. For example, for ingested devices, accurate localization as they travel through the gastrointestinal tract is essential as device telemetry will often need to be correlated with biogeographical information. Received signal strength indicator (RSSI) methods have been widely adopted for location determination. However, these approaches require multiple sensor nodes distributed outside of the body, recovering only the absolute location of the device with little information about its surrounding biological environment. Localization accuracy is also generally low (about 1 cm) [1], unsuitable for mm-scale devices. An alternative approach, pursued here, is to make the device trackable in an imaging system, while using the energy provided by the imager for power delivery and data telemetry.

In this work, we presents a custom data and power front-end for mm-scale implants which function while being imaged in an ultrasound brightness-mode (B-mode) imager. In this context, a single ultrasound transducer array operating as a traditional B-mode imager will power up many of these devices within its field of view (FOV), and each device's transmitted data is localizable with the reconstructed images. Although many implantable biomedical devices [2-3] use ultrasound for powering and data telemetry because of its low attenuation in tissue (1dB/cm/MHz) and high safety limits (7.2 mW/mm^2), none of them, to our knowledge, has shown compatibility with ultrasound medical imaging.

In a typical B-mode imaging application, elements in a piezoelectric transducer array are activated with programmed delays to generate a short, focused ultrasound pulse that travels into the tissue. The same transducer array is then used to record the reflected echo. The delay between the pulse and echo is proportional to the depth at which a reflecting acoustic impedance mismatch is found. A cross-section image is then generated by sweeping this focused pulse from the transducer array. This working principle provides an extremely low duty cycle for ultrasound energy at any one point within the FOV: shorter pulses are preferred for higher resolution, and with ideal beamforming, every location within the FOV receives only one such pulse per imaging frame. The chip in this work is designed to cold start and remain fully functioning with such low duty cycle power through a combination of ultra-low power consumption and active rectification.

To minimize the overall size of the implant, a single piece of lead zirconate titanate (PZT) piezoelectric transducer is used for energy conversion and bidirectional communication. Localization of multiple devices in the same FOV is further assisted by instructions implemented on-chip. The chip supports a digital controller and a simple instruction set which supports two powering modes: a default one compatible with imaging and one in which focused ultrasound energy is available after localization to provide more power to peripheral functions.

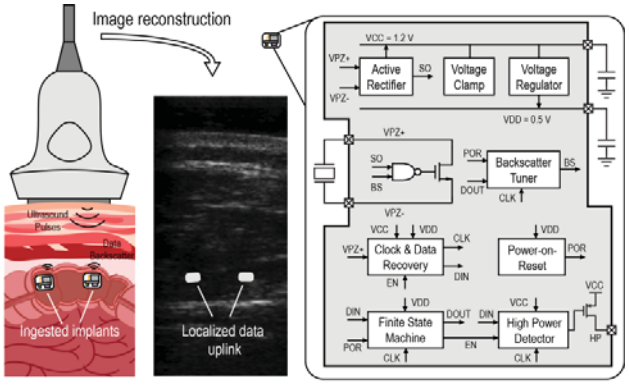

Fig. 1 Concept art and block diagram of the chip

* 978-1-5386-9395-7/19/$31.00 ©2019 IEEE

II. System Architecture

Fig. 1 depicts the localization of multiple chips within a single FOV in an ultrasound image. A B-mode imager running at 50 frames per second (FPS), serving as the host, sends pulses to scan a cross sectional area. The pulse width used for each frame is modulated between wide and narrow, for a pulse-width-modulated (PWM) digital data downlink, supporting a data rate of 50 bit/s. On the chip side, an active rectifier harvests the power from this extremely low duty cycle ultrasound energy through a PZT transducer as small as 1 mm by 1 mm by 0.5 mm, producing a V_{CC} of approximately 1.2 V. The clock-and-data-recovery (CDR) circuit synchronizes the clock on-chip to the frame rate and recovers data from PWM. A backscatter tuner circuit implements the backscatter pressure amplitude-shift-keying (ASK) uplink, which supports a data rate of 25 bit/s. A 0.5-V V_{DD} is generated from a voltage reference and a voltage regulator to power the rest of the digital logic. A custom ultra-low power digital standard cell library is used to implement the instruction set of the chip, shown in Table 1, with hardwired control. Power-on-reset ensures the correct initial state of all digital circuits. A high-power detector circuit is used to avoid potential deadlock if instruction "YIELD" is issued but no focused power is available to the chip. After the presence of focused power is confirmed, the chip then wakes up any integrated peripheral device and transfers harvested power to it.

A. Active Switch-Only Rectifier

Fig. 2 shows the electrical model of the PZT transducer (PZT-5A4E, Piezo Systems) as well as the schematic of the active switch-only rectifier [4]. Topologies achieving higher power enhancement ratios than switch-only usually require a bulky inductor or large switching capacitor array, which are incompatible with small-form-factor devices. Although active rectifiers generally achieve higher efficiencies than their passive counterpart, this is not necessarily the case when cold starting from extremely low-duty-cycle pulses; the static power consumption required for the comparator to function at MHz frequencies can be greater than the benefit it brings during the small fraction of time it is operating. In order to achieve an overall higher efficiency, the biases of M_{N1} and M_{N2} in the comparator are connected to V_{FBR}. In this manner, the comparator consumes more power than if statically biased when an ultrasound pulse is present but is turned off when no ultrasound is present, achieving a better trade-off point for low-duty-cycle operation.

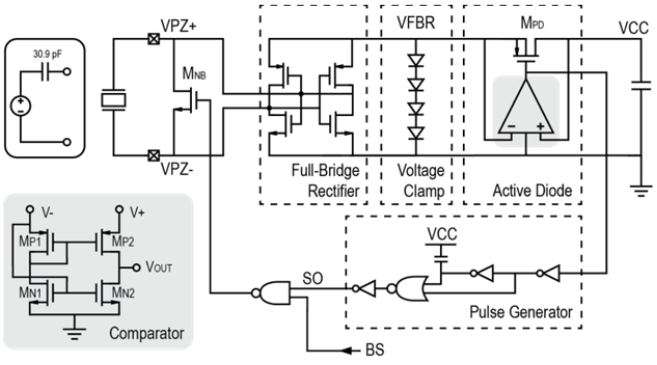

Fig. 2 Lumped model for PZT and topology of the active rectifier

B. Clock Recovery, Data Recovery and Backscatter Tuning

The clock recovery, data recovery, and backscatter modulation circuits are shown in Fig. 3. Imperfect beamforming from the B-mode imager transducer array may produce side lobes, creating a short train of pulses with varying amplitude at each single location, potentially corrupting clock synchronization and data recovery. In order to synchronize to the frame rate of the imager, a blackout period is generated to prevent the clock from being retriggered more than once within each frame. Pulse width is calculated with a four-bit counter counting the number of cycles of the ultrasound carrier in a pulse, and a shorter blackout period is used to avoid over-counting. In this manner, the data downlink rate is determined by the frame rate.

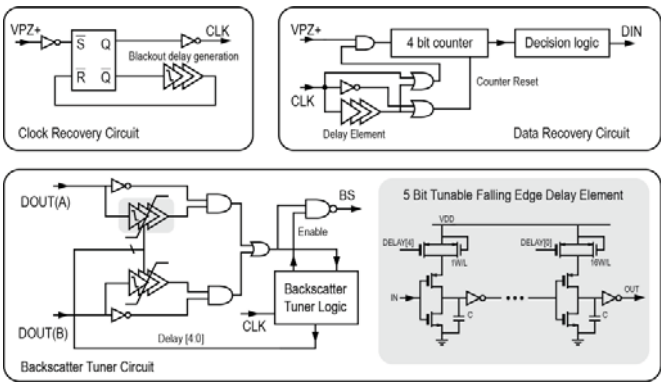

Fig. 3 Schematic of the clock recovery circuit, data recovery circuit, and backscatter tuner circuit

In order to achieve high backscatter ratios for the data uplink, when the backscattered data is "0", the two terminals of the transducer are effectively shorted, leaving no clock recovery to trigger the on-chip synchronized logic and leading to a potential deadlock. The backscatter tuning circuit solves this issue by flipping every "0" to "1" appearing on node *BS* after a certain delay, which is determined by a five-bit tunable falling edge delay element tuned to approximately one clock cycle long, such that only one frame will see the "0" for every "0" sent by the chip. Clock recovery will resume on the next frame. In addition, two approaches are used to maintain a constant uplink data rate independent of a missing clock cycle after every "0". First, all bit "1"'s are extended by one clock cycle such that the bit time for "1" is two frame periods. Second, an additional matched data path *DOUT(B)* is used in parallel with the main data path *DOUT(A)*. In the case of consecutive "0"'s on the uplink, *DOUT(A)* holding at "0" will not turn *BS* to "0" again. Instead, when sending a second "0", *DOUT(A)* will flip back to "1" and this "0" is passed to *DOUT(B)*. Every consecutive "0" will be sent alternatively between the two data paths. The bit time for both "1" and "0" are thus exactly two clock cycles, effectively with a "1" appended to each bit, yielding a constant uplink data rate at one half the frame rate of the imager.

C. Data Packet Structure and Instructions

A hardwired finite state machine is used to implement the protocol and instruction set shown in Table 1. The uplink data packet has headers for recognition. A parity-check bit and its inverse are included in each frame to improve uplink reliability as well as to indicate the end of the frame. Eight-bit, one-time programmable fuses are included on chip to give each device a unique identification (ID). Except for the instruction "QUERY ID", the chip will only respond to instructions sent with the appropriate ID, allowing parallel operation of multiple devices without interference.

TABLE I. PACKET STRUCTURE AND INSTRUCTION SET

Data downlink protocol				
Bit range	[15:12]	[11:8]	[7:0]	
Data	0101	INST	ARG	
Comment	Header	4 bit code for instruction	Argument of the instruction	
Data uplink Protocol				
Bit range	[15:14]	[13:10]	[9:2]	[1:0]
Data	00	INST	RET	Parity and its inverse
Comment	Header	Received instruction	Return value	Also marks the end of the frame
List of instructions				
Name	INST	ARG	RET	Comment
QUERY ID	0101	Do not care	ID	Return device's ID
HELLO	0110	ID	HELLO	HELLO = 01010101
CONFIG	1010	ID	ACK	ACK = 10101010
SAVE	1001	DATA	ACK	Only works if previous instruction is CONFIG
LOAD	1100	ID	DATA	
YIELD	1101	ID	ACK	

III. MEASUREMENT RESULTS

The chip is fabricated in a 180-nm technology occupying a total area of 740 µm by 830 µm, including the pad frame and custom ultra-low-leakage electrostatic discharge (ESD) protection devices. With only 10 pads, the chip is flip-chip packaged on a custom PCB with two 0201 capacitors and one 1-mm-by-1-mm-by-0.5-mm PZT transducer, passivated in polydimethylsiloxane (PDMS), achieving a total volume of 11 mm^3 (Fig. 4). Electrical testing shows a minimum static power consumption of 57 pW at 1.2V V_{CC}.

The linear transducer array probe L12-3V from Verasonics is used for ultrasound testing, configured to generate a 12-mm-by-50-mm cross section image at 50 FPS. A 4-MHz center frequency is chosen as a trade-off between low attenuation and high resolution. A three-cycle-wide pulse is used as a bit "0" for data downlink, a five-cycle-wide pulse serves as bit "1", and a four-cycle-wide pulse is used for imaging and smooth power delivery. The effective energy duty cycle is around 50 ppm. Waveforms of the ultrasound pulses are measured using a hydrophone (Fig. 5a). Castor oil is used to emulate the acoustic loss in body tissue. Fig. 5b shows the rectifier output V_{CC} and regulated V_{DD} ramp up from cold start with 400 kPa ultrasound pulses broadcasting the "QUERY ID" instruction. Fig. 5c shows the waveforms of the recovered clock, data downlink, and data uplink. Time-domain waveforms of the reflected echoes are recorded using the L12-3V transducer array at 16 MSamples/s as shown in Fig. 5d. A maximum 19% echo intensity difference is observed between different backscatter states. Echo pressure within the FOV is then plotted across frames for device identification. An example of this is shown in Fig. 5e; in response to a "QUERY ID" from the imager, the chip returns its ID "0xFF". An effective E_b/N_0 can be defined for the backscatter pressure ASK. The geometric center of the E_b/N_0's spatial 3dB cut-off region has been found to be a good indicator of the location of the device, with 0.8 mm accuracy characterized from experiments done with the device placed at 8 different known locations.

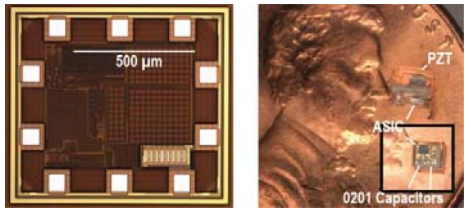

Fig. 4 Chip micrograph and photo of the fully packaged device

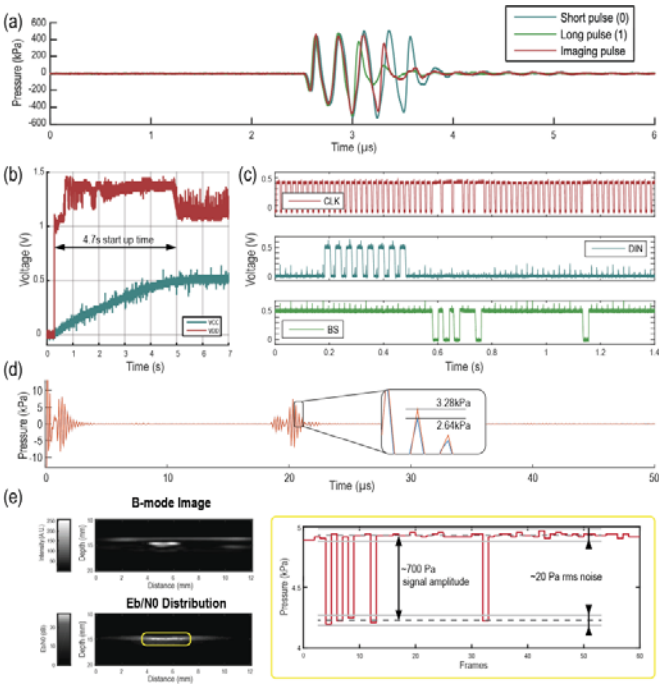

Fig. 5 Waveforms illustrating the functionality of the chip. (a) Pressure pulses measured by a hydrophone, (b) V_{DD} and V_{CC} ramp up during cold start up, (c) chip recovered clock, recovered data, and backscatter signal, (d) time domain waveform of the echo, and (e) reconstructed B-mode image, its E_b/N_0 distribution, and pressure changes across frames.

Fig. 6 shows the test setup for *in vitro* measurements, where chicken thighs are used as animal tissue layers. Two devices are sandwiched between layers of tissue at different depths, while immersed in castor oil. The imager array powers up both devices simultaneously. Although accurate alignment is impossible, making direct localization on the reconstructed image difficult, their data signatures are still robustly captured and well localized. Both devices respond to "QUERY_ID" at the same time with their ID being "0xFE" and "0xFF"

respectively. The imager then exchanges the "HELLO" instruction with the two devices individually without any interference observed.

In order to verify power delivery capability, simulated ultrasound pulses are programmed to issue a "YIELD" instruction after initial data exchanges. A 0.5% duty cycle pulse is used to mimic high power delivery with a 100 pF in parallel with 5 MΩ as the load on the *HP* pin. Fig. 7 shows the time domain waveforms at *HP* during power mode switching. A 3 ms delay is observed before the chip confirms the presence of a higher duty cycle power delivery. 280 nW of power is delivered to the load.

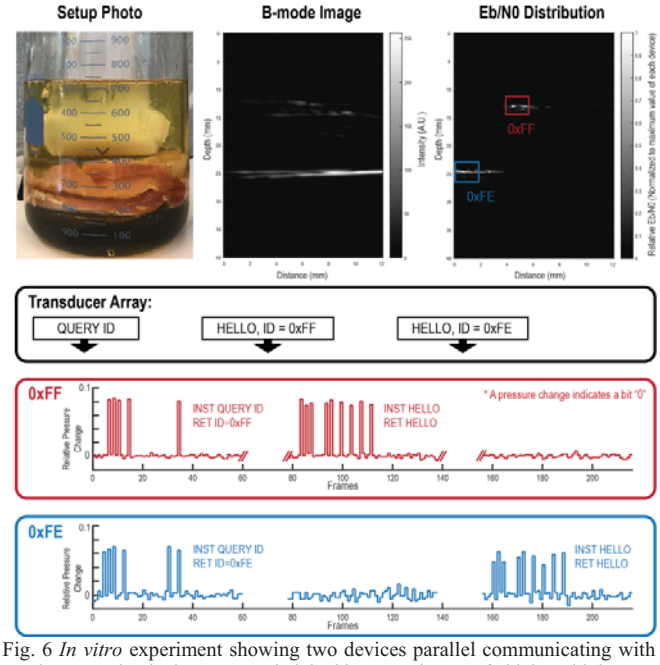

Fig. 6 *In vitro* experiment showing two devices parallel communicating with one imager. The devices are sandwiched between layers of chicken thighs.

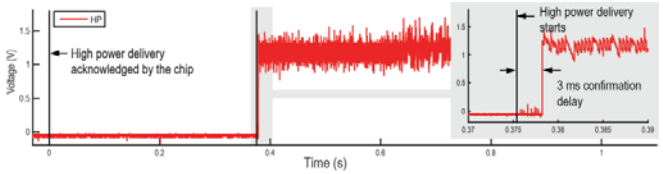

Fig. 7 Time domain waveform of node *HP* during switched power delivery.

Fig. 8 shows the measured and theoretical minimum pressure at the surface of the tissue needed to power up the chip as a function of depth. Mechanical index (MI) is another safety requirement which limits pulsed ultrasound, defined as $PNP/(F_C)^{0.5}$, where PNP is the peak negative pressure and F_C is the center frequency. For pulsed operation, MI must generally be kept below 1.9 $MPa/(MHz)^{0.5}$. E_b/N_0 is also reported as a function of device depth. The results show reliable power delivery and data communication down to 40 mm and predict a maximum implant depth of 71 mm with good alignment.

IV. Conclusion

This work has demonstrated the first chip that enables deep tissue devices to harvest power and establish bi-directional data links with a single imaging-mode ultrasound transducer array. Through ultrasound B-mode imaging, the implants can be individually localized with sub-mm-level accuracy in real time by their distinct data signature, within a cross-section image that also carries information about their surrounding environment. The low power and high backscatter ratio enables a maximum implantation depth of 71 mm, and with at least 280 nW power delivery capability for *in vivo* biological measurements. Table 2 shows a comparison between this work and other deep tissue implants using different mechanisms.

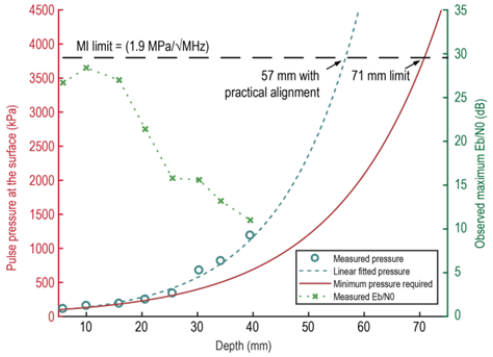

Fig. 8 Pulse pressure required at the surface for increasing implant depth, with E_b/N_0 reported at depth measured.

TABLE II. Comparison with Related Works

	[1]	[2]	[3]	**This Work**
Technology	65 nm	65 nm	180 nm	**180 nm**
Power modality	Battery	Ultrasound	Ultrasound	**Ultrasound**
Tracking mechanism	RSSI	N/A	N/A	**Ultrasound imaging**
Localization accuracy	9.8 mm	N/A	N/A	**0.8 mm**
Number of transducers	8	2 (1TX / 1RX)	2 (1TX / 1RX)	**1**
Data downlink	RF OOK	Ultrasound Edge Detection	Ultrasound OOK	**Ultrasound PWM**
Data uplink	RF QPSK / BPSK	Ultrasound backscatter	Ultrasound OOK	**Ultrasound backscatter**
Implant depth	> 300 mm	21.5 mm	85 mm	**71 mm**
Implant size	3620 mm^3	6.5 mm^3	30.5 mm^3	**11 mm^3**

Acknowledgment

This work was supported in part by a grant from the W. M. Keck Foundation.

References

[1] J. Jang et al., "4-Camera VGA-resolution capsule endoscope with 80Mb/s body-channel communication transceiver and Sub-cm range capsule localization," 2018 IEEE International Solid - State Circuits Conference (ISSCC), San Francisco, CA, 2018, pp. 282-284.

[2] B. C. Johnson et al., "StimDust: A 6.5mm3, wireless ultrasonic peripheral nerve stimulator with 82% peak chip efficiency," 2018 IEEE Custom Integrated Circuits Conference (CICC), San Diego, CA, 2018, pp. 1-4.

[3] T. C. Chang, M. L. Wang, J. Charthad, M. J. Weber and A. Arbabian, "27.7 A 30.5mm3fully packaged implantable device with duplex ultrasonic data and power links achieving 95kb/s with <10−4BER at 8.5cm depth," 2017 IEEE International Solid-State Circuits Conference (ISSCC), San Francisco, CA, 2017, pp. 460-461.

[4] Y. K. Ramadass and A. P. Chandrakasan, "An Efficient Piezoelectric Energy Harvesting Interface Circuit Using a Bias-Flip Rectifier and Shared Inductor," IEEE Journal of Solid-State Circuits, vol. 45, no. 1, pp. 189-204, Jan. 2010.